Materials Today Communications 37 (2023) 107509

Contents lists available at ScienceDirect

Materials Today Communications

journal homepage: www.elsevier.com/locate/mtcomm

Design of silver containing mesoporous bioactive glass-embedded polycaprolactone substrates with antimicrobial and bone regenerative properties

Valentina Peluso [a,1], Ugo D'Amora [a,*,1], Ana Maria Prelipcean [b], Stefania Scala [c], Nicola Gargiulo [d], Ana-Maria Seciu-Grama [b], Domenico Caputo [e,f], Roberto De Santis [a], Antonio Gloria [a,g], Teresa Russo [a,*]

[a] Institute of Polymers, Composites and Biomaterials - National Research Council of Italy, V. le J. F. Kennedy 54, Mostra d'Oltremare, Pad. 20, 80125 Naples, Italy
[b] Department of Cellular and Molecular Biology, National Institute of Research and Development for Biological Sciences, 296 Splaiul Independentei, Bucharest 060031, Romania
[c] Department of Biology, University of Naples Federico II, Via Cinthia, Naples 80126, Italy
[d] CeSMA, Advanced Metrological and Technological Services Center, University of Naples Federico II, Corso N. Protopisani, Napoli 80146, Italy
[e] ACLabs, Applied Chemistry Laboratories, Department of Chemical, Materials and Production Engineering, University of Naples Federico II, P.le V. Tecchio 80, Napoli 80125, Italy
[f] INSTM, National Interuniversity Consortium of Materials Science and Technology, Via G. Giusti, 9, Firenze 50121, Italy
[g] Department of Industrial Engineering, University of Naples Federico II, P.le Tecchio 80, 80125 Naples, Italy

ARTICLE INFO

Keywords:
Design of composite substrates
Mesoporous bioactive glasses
Silver
Polycaprolactone
Mechanical analysis
Bone tissue engineering
Antibacterial properties

ABSTRACT

Objectives: The aim of the present study was to design, produce and characterize composite substrates consisting of different formulations of poly(ε-caprolactone) (PCL), as a polymer matrix, and silver-containing mesoporous bioactive glasses (Ag-MBGs) with improved properties for bone tissue engineering.
Methods: Ag-MBGs were synthesized by an evaporation-induced self-assembly process. Different polymer-to-particles weight ratios were considered (90/10, 80/20, 70/30 w_t%). PCL/Ag-MBGs composites substrates were manufactured by melting and molding technique. The effect of Ag-MBGs embedded in the polymer matrix was investigated by morphological (field emission scanning electron microscopy (FE-SEM), SEM and contact angle measurement), structural/functional (small punch and tensile tests), antimicrobial, and *in vitro* biological analyses.
Results: The obtained results highlighted that the inclusion of 10% by weight of Ag-MBGs improved the punching performances as well as the tensile Young's modulus (from 350.3 ± 32.0 MPa for PCL to 473.5 ± 41.0 MPa), without negatively altering the tensile strength of the neat PCL. Indeed, small punch test findings indicated that, over a threshold concentration (10% by weight), the Ag-MBGs acted as "weak points", rather than reinforcement, because the mechanical properties of the composite substrates decreased. The bacterial growth monitoring showed a clear antimicrobial effect against both Gram-negative and Gram-positive, confirmed by reduced cell viability registered after 24 h (2×10^5 CFU/mL for *P. aeruginosa* and 2.3×10^5 CFU/mL for *S. aureus*). The results were confirmed in terms of adhesion and adherent growth, reduced at day 3 on PCL samples with 10% of Ag/MBGs. Furthermore, this formulation induced a significant inhibition zone (21 mm for *P. aeruginosa,* 23 mm for *S. aureus*). *In vitro* biological assays confirmed that all formulations of PCL/Ag-MBGs supported periodontal ligament stem cells' viability and differentiation over time. Particularly, substrates with Ag-MBGs at a concentration of 10% and 20% by weight of Ag-MBGs provided higher values of the percentage of Alamar Blue reduction meanwhile, the highest Ag-MBGs concentration induced a higher expression of alkaline phosphatase activity.
Significance: Ag-MBGs proved to be suitable candidates as filler at a specific threshold concentration (10% by weight), considering a compromise among physicochemical, antimicrobial, and pro-regenerative features. These

* Corresponding authors.
E-mail addresses: ugo.damora@cnr.it (U. D'Amora), teresa.russo@cnr.it (T. Russo).
[1] Both authors equally contributed to this work

https://doi.org/10.1016/j.mtcomm.2023.107509
Received 22 May 2023; Received in revised form 11 October 2023; Accepted 2 November 2023
Available online 5 November 2023

findings provide useful data for the design and development of improved biomaterials with optimized properties, suggesting a potential application in maxillofacial bone and/or periodontal tissue repair.

1. Introduction

Bone diseases, such as congenital anomalies, osteoporosis, periodontitis, bone bacterial infections (i.e., osteomyelitis), or injuries as a result of trauma are among the most common causes of abnormalities of the human skeletal system. In this scenario, the design of substrates as membranes and scaffolds for guided bone tissue engineering has boosted great progress in material science and technology. Indeed, regenerative medicine has shown the ability to overcome the limitations associated with current treatments. As reported in the literature, over the past years, different polymer-based composites for bone tissue engineering have been developed and many approaches aiming at improving their performances have been adopted [1–3]. Specifically, controlled biodegradability and bioresorbability, porosity, optimized mechanical, and mass transport properties, as well as surface topography and chemistry remain the most prominent features to favor cell adhesion, proliferation, and differentiation. It is worth noting that bone tissue-engineered scaffolds must also be bioactive, a key property to promote osseointegration through the formation of a layer of hydroxyapatite (HAp) [4,5]. From a material point of view, several kinds of materials (synthetic, natural, semi-synthetic, and hybrid) and different technological approaches have been properly adopted to design and manufacture bone tissue-engineered scaffolds for *ex vivo* approaches [6–8]. Ceramic materials are brittle and do not properly match the mechanical performances of natural bone, even if they often resemble its inorganic phase. On the other hand, differently from natural polymers, synthetic polymers may possess tailorable properties as their physicochemical properties, degradation rate, and mechanical performances can be suitably modulated by varying the chemical composition or structure of the macromolecule. In particular, synthetic aliphatic polyesters such as polyglycolic acid, polylactic acid, and their copolymers and poly (ε-caprolactone) (PCL) have been widely investigated [9]. Nevertheless, synthetic materials lack in terms of bioactivity and they cannot fully recapitulate the bone tissue.

For this reason, research attention has been focused on the possibility to combine biodegradable polymers and inorganic phases (ceramic micro/nanoparticles) as a promising approach to develop composite materials. If compared to polymeric structures, polymer-based composites show improved physicochemical, mechanical, and biological properties.

Among the inorganic phases, a growing interest has been driven towards the synthesis of highly ordered mesoporous bioactive glasses (MBGs) characterized by high specific surface area and pore volume, and greatly enhanced bone-forming bioactivity as compared with conventional BGs, essentially due to their unique textural and structural properties [10–18]. In particular, nanostructured mesoporous siliceous materials represent ordered systems of pores with a uniform size (between 2 and 50 nm), useful also as drug delivery systems [19–21]. Owning to the possibility to combine their ability to deliver drugs with radiotherapy, photothermal therapy, and magnetic hyperthermia, MBGs have also shown promising for anticancer therapies. Furthermore, they have demonstrated high bioactivity, biocompatibility, and osteoconductive properties that can be probably ascribed to their highly-ordered structure [22,23]. They possess a similar composition to traditional bioactive glass (SiO_2-CaO-P_2O_5) but exhibit higher bioactivity. Furthermore, a HAp apatite layer on the surface of MBGs can be formed after short reaction times and soaking in simulated body fluids (SBFs) [24]. It has also been demonstrated that Ca^{2+} and Si^{4+} ions can stimulate osteoblast proliferation and differentiation, thus suggesting MBGs as potential candidates for bone tissue regeneration [25]. Recently, silver-containing mesoporous bioactive glasses (Ag-MBGs) have been also developed as the silver inclusion could improve their biological, textural, and antibacterial activity [26]. The increasing number of implanted medical devices has revolutionized the quality of life of patients, nevertheless, implant-associated infections remain a common and severe complication in the biomedical field. *Staphylococcus aureus (S. aureus)* is one of the most common causes of biomaterial-related infection. Upon attachment to the biomaterial, these bacteria proliferate and develop dense communities encased in a protective matrix, called biofilm. *Pseudomonas aeruginosa* (*P. aeruginosa*) as well, causes serious therapeutic problems because of its multidrug resistance [27]. A local antibiotic delivery into damaged bone as bone infection therapy may allow: high drug concentration at the diseased site, prolonged and controlled drug delivery, and the reduced adverse side effects of the systemic doses, overcoming the limits of antibiotherapy in terms of efficacy and feasibility [28,29]. Furthermore, targeted delivery offers promising perspectives, especially for multidrug resistant strains. For example, Zhao et al. [24] demonstrated that Ag-MBGs could release Ag^+ ions in deionized water and SBF in a sustained manner, exhibiting an antimicrobial effect against planktonic cells of *Escherichia coli (E.coli)*. In a previous work, Gargiulo et al. [21] highlighted that Ag-MBGs, obtained by evaporation induced self-assembly and successive thermal stabilization, showed a well-ordered array of 1D mesoporous channels, as shown by transmission electron microscopy images and a bacteriostatic/bactericidal effect against *S. aureus* strain, with strong evidence of bactericidal activity already registered at 0.5 mg/mL of glass concentration [21]. In particular, the bioactivity of the Ag-MBGs was assessed in Dulbecco's Modified Eagle Medium (DMEM) solution instead of the Kokubo's SBF, evidencing the DMEM-mediated transformation of a MBG into carbonate-substituted HAp [21]. The antibacterial activity of Ag-MBGs against *Enterococcus faecalis* biofilm in root canal was also reported by Fan et al. [25].

Accordingly, the current research aimed at developing composite substrates consisting of a PCL matrix and Ag-MBGs with improved properties, bactericidal and pro-regenerative behavior, for bone tissue engineering applications. The effect of Ag-MBGs embedded in the polymer matrix was evaluated by preliminary structural/functional, microbiological tests and biological analyses.

2. Materials and methods

2.1. Chemicals

Pluronic P123, tetraethyl orthosilicate (TEOS), calcium nitrate tetrahydrate ($Ca(NO_3)24\ H_2O$), triethyl phosphate (TEP), silver nitrate ($AgNO_3$), ethanol (EtOH) were from Sigma Aldrich (Milan, Italy) except for nitric acid (HNO_3), supplied by Fisher Scientific (Milan, Italy), and ultra-purified water, which was produced using a TKA Smart2Pure device (Thermo Scientific, Waltham, MA, United States). All these reagents were used for the synthesis of Ag-containing bioactive glasses (Ag-MBGs).

Poly(ε-caprolactone) (PCL) and tetrahydrofuran (THF) were from Sigma Aldrich (Milan, Italy) and used for substrate preparation.

S. aureus (ATCC 25923) and *P. aeruginosa* (ATCC 27853) were obtained from the American Type Culture Collection (ATCC, Manassas, VA, United States) for the microbiological tests. Phosphate-buffered saline (PBS), methanol, crystal violet solution, and acetic acid were from Sigma Aldrich (Saint Louis, MO, United States).

Periodontal ligament stem cells (PDLSCs) were supplied by Magna Græcia University of Catanzaro and adopted for substrate *in vitro* validation. Dulbecco-modified Eagle's medium high glucose (DMEM) with

and without Phenol red, trypsin/ethylene diamine tetraacetic (EDTA), formaldehyde, rhodaminate phalloidin (Atto Rho6G phalloidin) and 4',6-Diamidino-2-phenylindole (DAPI) were from Sigma Aldrich (Darmstadt, Germany). Fetal bovine serum (FBS) from Gibco, Thermo Fisher Scientific (Waltham, MA, United States). L-glutamine, penicillin G sodium, antibiotic/antimycotic, and streptomycin from Euroclone (Milan, Italy).

2.2. Synthesis of Ag-containing mesoporous bioactive glasses (Ag-MBGs)

The synthesis of Ag-MBGs was obtained by adapting one of the protocols reported in the literature for the production of non-Ag-enclosing MBGs [21]. Briefly, pluronic P123 (4.0 g), TEOS (6.7 g), Ca $(NO_3)24\ H_2O$ (1.4 g), TEP (0.73 g), $AgNO_3$ (0.117 g) and 0.5 M HNO_3 (1.0 mL) were dissolved in EtOH (60 g) and stirred at room temperature for 1 day. The resulting solution was introduced into a Petri dish and underwent an evaporation-induced self-assembly (EISA) process. The dried gel was calcined at 500 °C for 5 h. Coarse particles of Ag-MBG were ground into fine powders and sieved through a 600 μm-mesh sieve.

2.3. Morphological characterization

Field emission scanning electron microscopy (FE-SEM) micrographs were collected with a Zeiss Ultra Plus instrument (Oberkochen, Germany). For the elemental analysis and assessment of the particle composition, the instrument was equipped with an Oxford x-act detector for energy dispersive spectroscopy (EDS).

2.4. Substrate preparation

PCL/Ag-MBG substrates were manufactured by embedding Ag-MBGs into a PCL matrix. At room temperature, PCL (M_w=65 kDa) pellets were dissolved in THF, under magnetic stirring. A PCL:THF ratio of 80:20 (w/w) was used. Ag-MBGs were gradually added to the PCL/THF solution during stirring, until the desired amounts of polymer-to-particles weight ratios of 90/10, 80/20, and 70/30 w_t%, respectively, were reached. To optimize the particle dispersion and avoid clustering in the polymer solution, an ultrasonic bath (Branson 1510 MT, Danbury, CT, United States) was also employed for 30 min before precipitation. Afterward, the addition of EtOH allowed the precipitation of a composite paste that was pelletized. Neat and composite pellets were melted at 120 °C and by melting and molding technique miniature disc-shaped specimens (Ø = 6.4 mm; h= 0.5 mm) and tensile samples, in the form of a dogbone, were manufactured (Fig. 1). Starting from now on and throughout the manuscript, PCL will indicate the neat polymeric substrate, while PCL/Ag-MBG 90/10, 80/20, and 70/30 will denote the composite substrates.

2.5. Morphological analysis and contact angle measurements

SEM was employed to assess the morphology of PCL/Ag-MBG composites using FEI Quanta FEG 200 apparatus (Hillsboro, OR, United States of America).

For sample preparation, substrates were coated with an ultrathin layer of Au/Pt by using an ion sputter and observed by SEM.

Surface wettability was evaluated by the apparent water contact angle measurements. The contact angle measurements were conducted on PCL and PCL/Ag-MBGs substrates at different Ag-MBGs loadings, by sessile drop method with an automatic drop shape analysis system DATAPHYSICS OCA 20 apparatus (DataPhysics Instruments GmbH, Filderstadt, Germany). Briefly, distilled water (0.25 μL) was dropped onto different sites on each specimen and the static contact angle was evaluated. The apparent contact angle was calculated as an average of ten measurements.

2.6. Mechanical analysis

2.6.1. Small punch test

PCL and PCL/Ag-MBGs were immersed in a physiological solution at 37 °C. Small punch tests were performed on disc-shaped specimens, according to the ASTM F2183 standard, thus evaluating the maximum load and the displacement at maximum load. All the tests were conducted using an INSTRON 5566 testing machine (Bucks, UK). The experimental set-up consisted of a hemispherical head punch, to load axisymmetrically the specimen in bending at a constant displacement rate of 0.5 mm/min until failure occurred, a die, and a guide for the punch. The values of load and displacement were recorded during the test.

2.6.2. Tensile test

PCL and PCL/Ag-MBGs were immersed in a physiological solution at 37 °C. Tensile tests were conducted on PCL and PCL/Ag-MBG specimens using an INSTRON 5566 testing machine, according to the ASTM D1708 standard. The tensile modulus was calculated as the slope of the initial linear portion of the stress-strain curves. Toe compensation was properly made according to the standard test method. The values of maximum stress and strain were evaluated. However, it is worth noting that even though this test method cannot be employed for the determination of the modulus of elasticity, it was used to make a comparative analysis among the different samples which were assessed under the same conditions.

2.7. Microbiological analyses

2.7.1. The antibacterial activity on planktonic growth

The antibacterial activity of the scaffolds was evaluated on both Gram-positive, *S. aureus* (ATCC 25923) and Gram-negative strains, *P. aeruginosa* (ATCC 27853). Samples were sterilized by UV for 1 h on each side. *S. aureus* was grown on trypticase soy agar (TSA) nutrient medium and *P. aeruginosa* on Luria Bertani agar at 37 °C. The overnight culture was diluted to a final concentration of 1×10^8 colony forming units per mL (CFU/mL) in each well containing 2 and 4 mg/mL of PCL/

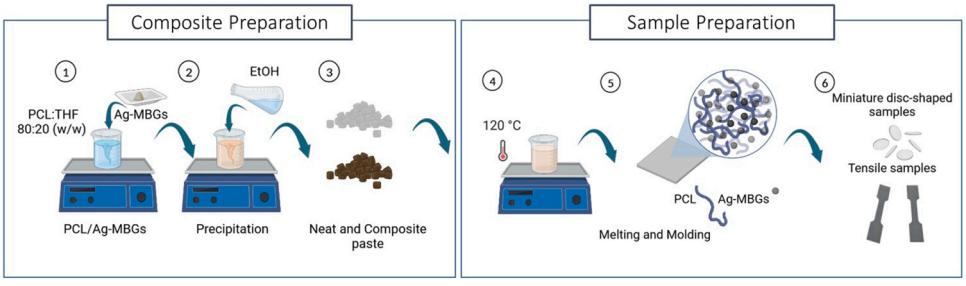

Fig. 1. Schematic representation of the production process for polycaprolactone/silver containing mesoporous bioactive glasses particles (PCL/Ag-MBGs) substrates. Composite preparation: 1) PCL/Ag-MBGs in THF, 2) ethanol (EtOH) precipitation, 3) neat and composite paste. Sample preparation: 4) melting and molding, 5) PCL/Ag-MBG sheet preparation, 6) punching of cylindrical samples for physicochemical, mechanical, microbiological, and biological analyses, and dogbone shape for tensile test.

Ag-MBGs extracts. After 1 and 3 days, the absorbance of the supernatant was assessed at 600 nm to determine the bacterial viability using a Sunrise microplate reader (Tecan, Männedorf, Switzerland). For the tested concentration of 4 mg/mL, microbial cell viability was also evaluated by assessing the number of colonies. Briefly, the sample was serially diluted starting from 10^{-1} to 10^{-7} and further plated on nutrient agar. Prior to evaluation, the seeded plates were incubated at 37 °C overnight and the number of colonies was counted, and the CFU/mL was estimated.

2.7.2. The antibacterial activity on biofilm formation

The antibacterial potential of the substrates against biofilm formation was spectrophotometrically evaluated by measuring the number of adhered bacterial cells. Briefly, bacterial suspensions were seeded at a density of 1×10^8 CFU/mL in each well in a 96-well plate. The number of bacteria from the two strains attached to the samples was spectrophotometrically measured. After 3 days, each substrate was washed three times in sterile PBS (pH 7.2) to remove planktonic cells, while the bacteria attached to the samples were fixed with methanol, stained with aqueous crystal violet 1% solution, and de-colored with acetic acid 33%. The optical density of each well stained with crystal violet was measured at 595 nm using a Sunrise plate reader.

2.7.3. Inhibition zone detection

As a first screening method, an adapted Kirby-Bauer assay was conducted on the two reference strains. Standardized bacterial suspensions corresponding to 0.5 McFarland density were prepared from fresh (24 h) solid cultures of the two bacterial strains. The samples were sterile disposed on the agar. The plates were incubated at 37 °C, for 24 h. After the incubation, the plates were photographed, and the diameter of the inhibition zone (mm) was measured using ImageJ software.

2.8. Biological analysis

2.8.1. Cell culture

According to previous research [30], periodontal ligament stem cells (PDLSCs) were cultured in DMEM, containing 10% (v/v) FBS, 200 mM L-glutamine, 100 U/mL penicillin G sodium and 100 mg/mL streptomycin, in a humidified atmosphere at 37 °C and 5% CO_2. The cells were subcultured using EDTA. Substrates for cell-culture experiments were prepared for cell seeding by soaking for 1 h in 70% EtOH and 1% antibiotic/antimycotic in PBS (2 h) and then pre-wetted in medium (2 h). PDLCs Cells (density 5.0×10^4 cells/sample), resuspended in 100 μL of medium/sample, were statically seeded onto the substrate.

2.8.2. Cell viability

Cell viability was evaluated using the Alamar Blue Assay (AlamarBlue™ Cell Viability Reagent, Invitrogen, USA). The assay is based on a redox reaction that occurs in the mitochondria of the cells; the reagent is modified by the reducing environment of viable cells, turns color, and becomes highly fluorescent. Color changes and increased fluorescence can be spectrophotometrically detected, using absorbance (detected at 570 and 595 nm) as a measure of cell viability. After 1, 3, 7, 14, 21, and 28 days from cell seeding, the cell-constructs were rinsed with PBS and, for each sample, 200 μL of DMEM without Phenol Red containing 10% (v/v) Alamar Blue was added, followed by incubation in 5% CO_2 diluted atmosphere for 4 h at 37 °C. 100 μL of the solution were subsequently removed from the wells and transferred to a new 96-well plate. The optical density was immediately measured with a Sunrise microplate reader at wavelengths of 570 and 595 nm. The number of viable cells correlates with the magnitude of dye reduction and is expressed as a percentage of Alamar Blue reduction, according to the manufacturer's protocol.

2.8.3. Cell differentiation

Alkaline phosphatase (ALP) is an important marker for the early state of osteogenic differentiation in staminal cells. A specific enzymatic assay (Alkaline Phosphatase Activity Assay Kit PNPP method, Elabscience, TX, United States) was used to evaluate the ALP activity (U/gprot). Under alkaline conditions, alkaline phosphatase catalyzes the hydrolysis of p-nitrophenyl phosphate disodium to produce p-nitrophenol and phosphoric acid. Under strong alkaline conditions, p-nitrophenol is bright yellow and has a maximum absorption peak at 405 nm. PDLSCs were seeded into 96-well plates (density of 5.0×10^4 cells). According to manufacturer instructions, at 7, 14, 21, and 28 days from seeding, cells were washed twice in PBS and lysed in 1 mL of lysis buffer. After collecting and centrifuging, the supernatant was used to calculate ALP. After a 30 min incubation with para-Nitrophenyl phosphate (pNPP), the phosphatase was completely inhibited by NaOH and the pNPP liberating inorganic phosphate and the conjugate base of para-nitrophenol (pNP). The ALP activity was directly proportional to the amount of 1 μmol p-nitrophenol produced by 1 g cell protein per minute catalyzing the substrate at 37 ℃ is defined as 1 activity unit, according to Eq. 1:

$$ALP \quad activity \quad \left(\frac{U}{gprot}\right) = \left[\frac{(\Delta A - b)}{aT}\right] \frac{f}{Cpr} \tag{1}$$

where ΔA is the absolute OD ($OD_{sample} - OD_{blank}$), b the intercept of the standard curve, a the slope of the standard curve, f the dilution factor of the sample before the test, T is the reaction time, Cpr is concentration of protein in the sample (gprot/L). ALP activity was normalized to total cellular protein using a colorimetric assay (Protein Assay, Bio-Rad Laboratories, Inc., Hercules, CA). In a 96-well microplate, 200 μL of dye reagent and 1 μL of sample were combined and the absorbance was measured at 595 nm.

2.8.4. Immunofluorescence studies

For the immunofluorescence study, PDLSCs seeded samples for 7, 14, 21, and 28 days were plated on 96-well, fixed with 4% formaldehyde in water for 1 h, washed with PBS, and immunostained with the Atto Rho6G phalloidin, for the F-actin filaments, and with DAPI, for the nuclei. The fluorescent signals were visualized using a fluorescence microscope (JuLI Stage Real-Time CHR, Cell History Recorder, NanoEn TecK. Inc. (HQ), Seoul, Republic of Korea) with a 20 X objective.

2.9. Statistical analysis

Each experiment was repeated at least three times in triplicate unless otherwise stated. Results are presented as mean ± standard deviation of independent measurements. Statistical analysis was performed by one-way or two-way ANOVA, followed by Bonferroni test with multiple comparisons among the distinct groups, by using GraphPad Prism software (version 7.0). The result may be evaluated as statistically significant considering different confidence levels (95–99.9999%).

3. Results

3.1. Synthesis and characterization of Ag-MBGs

Ag-MBGs were successfully synthesized following the procedure described by Gargiulo et al. [21]. The morphological analysis by FE-SEM revealed a smooth and homogeneous surface of the Ag-MBGs, as usually expected for glasses (Fig. 2a). The chemical composition obtained by EDS is reported in Fig. 2b, clearly highlighting all the characteristic elements of the synthesized BGs.

3.2. Mechanical and morphological characterization of PCL/Ag-MBGs

Regarding the mechanical characterization, small punch and tensile tests were performed on neat and composite materials. Furthermore, a

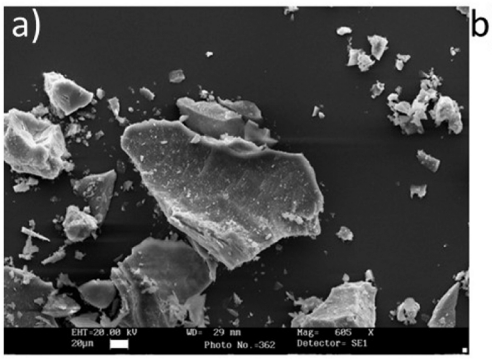

b)

Element	App Conc.	Intensity Corrn.	Weight %	Weight % Sigma	Atomic %
O K	33.45	0.3859	55.13	2.38	71.49
Si K	40.85	0.8573	30.30	1.66	22.38
P K	1.33	0.9171	0.92	0.60	0.62
Ca K	12.14	0.8722	8.85	0.68	4.58
Ag L	5.13	0.6796	4.80	0.88	0.92
Totals			100.00		

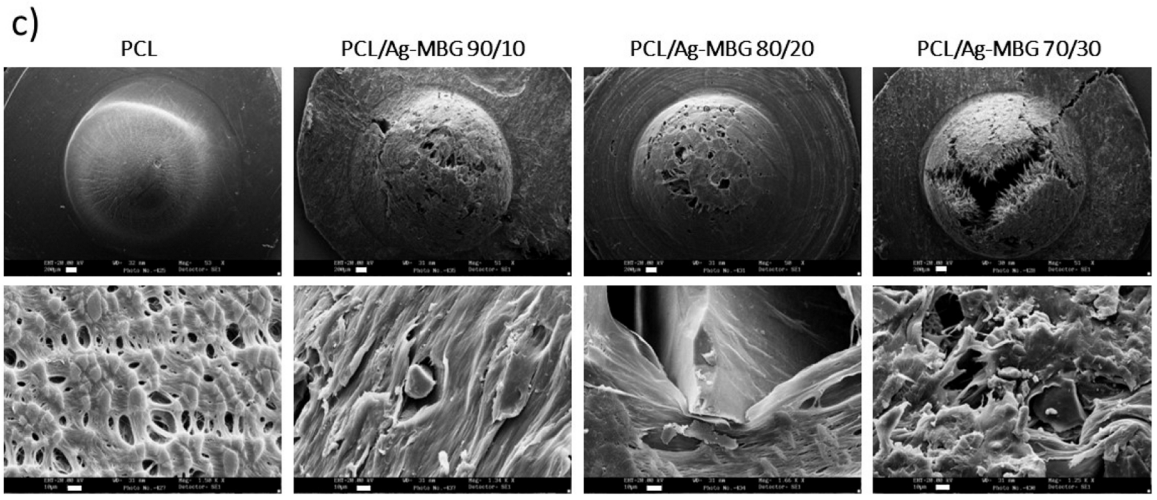

Fig. 2. a) Field emission scanning electron microscopy (FE-SEM) image of Ag-MBGs. Scale Bar: 20 µm. b) Energy dispersive X-ray spectroscopy (EDS) analysis. c) Scanning Electron Microscopy (SEM) images of punched PCL and PCL/Ag-MBGs substrates. Scale Bar: 200 µm (top), 10 µm (down).

morphological analysis was also performed on the punched samples (Fig. 2c). Representative curves obtained from small punch and tensile tests are reported in Fig. 3a and b, respectively.

3.2.1. *The small punch test*

The following analysis was chosen to assess the performances of the proposed disc-shaped PCL/Ag-MBG composite substrates, as it may be considered as a reproducible miniature test method, already employed to evaluate the mechanical properties of retrieved acrylic bone cement, PCL reinforced with sol–gel synthesized organic–inorganic hybrid fillers [31] or iron-doped HAp nanoparticles [32]. Load–displacement curves from small punch tests on PCL and PCL/Ag-MBGs composites showed an initial linear region, followed by a decrease in the curve slope until a maximum load was reached. Finally, a decrease in the load was evident until failure occurred for all the samples (Fig. 3a). Specifically, the inclusion of 10% by weight of Ag-MBGs represented an effective reinforcement, providing values of peak load (66.4 ± 6.2 N) that were higher than those obtained for the neat PCL substrates (51.1 ± 5.1 N), (Fig. 3c). The observed differences were statistically significant ($^{\S}p < 0.0001$). However, the different Ag-MBGs concentrations did not influence the displacement at the maximum load, which resulted similar to that shown by neat substrates (1.2 ± 0.3 mm) (Fig. 3d).

3.2.2. *The tensile test*

On the other hand, regarding tensile tests, Fig. 3b shows typical stress-strain curves for PCL and PCL/Ag-MBGs composites. The values of tensile modulus and maximum stress are reported as mean value ± standard deviation. In particular, the inclusion of 10% by weight of Ag-MBGs significantly improved tensile modulus (from 350.3 ± 32.0 MPa for PCL to 473.5 ± 41.0 MPa, $p < 0.001$) (Fig. 3e), without negatively altering the maximum stress, if compared to the neat PCL substrates (Fig. 3f). Anyway, by further increasing the filler concentration, the tensile modulus increased (up to 669.5 ± 50.2 MPa for PCL/Ag-MBG 70/30), whereas a decrease of the maximum stress was well evident (7.3 ± 0.8 MPa for PCL/Ag-MBG 70/30). In addition, it is worth noting that the increasing amount of Ag-MBGs strongly reduced the maximum strain (Fig. 3e).

3.2.3. *SEM analyses*

SEM of PCL-based composites evidenced that, in general, Ag-MBGs were properly embedded and uniformly distributed in the matrix. Furthermore, the presence of bioactive particles drastically modified the morphology of the substrates, reducing the ductility of the materials (Fig. 3c), as especially evidenced by tensile tests (Fig. 3b). However, SEM analyses on the punched PCL/Ag-MBGs composites also suggested that an increase of the Ag-MBGs concentration did not cause a brittle fracture, as evidenced by the presence of multiple frays of the polymer matrix (Fig. 2c).

Contact angle measurements. The hydrophilicity of the composite surface at varying filler loadings was assessed by measuring the static contact angle. Then, the obtained results were compared with those obtained from the neat PCL structures. The water contact angle of the PCL/Ag-MBGs substrates was lower than that of the neat PCL ones, thus suggesting that the presence of the inorganic fillers induced a more hydrophilic behavior. Particularly, the obtained values ranged from 85.3 ± 4.1° for the neat PCL substrates to 68.8 ± 5.3° for the PCL/Ag-MBGs composites. By varying the filler amount, any significant differences were observed. For all samples, the contact angle values were below 90°, showing a hydrophilic tendency [33].

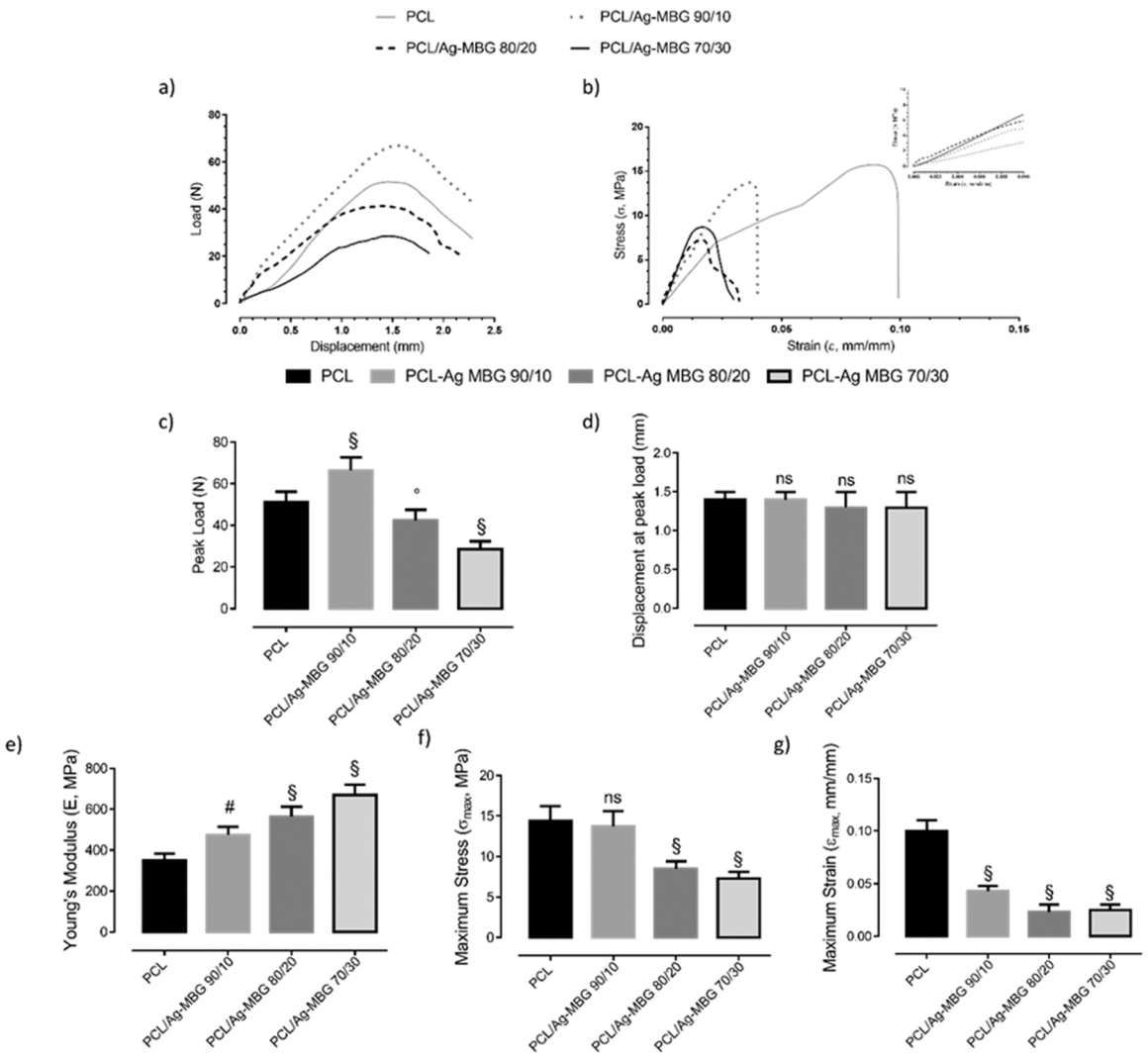

Fig. 3. Typical curves obtained by a) small punch tests and b) tensile tests performed on PCL and PCL/Ag-MBG composites. Results from mechanical analyses: c) and peak load and d) displacement at peak load, obtained from test a); e) tensile Young's modulus, f) maximum stress and g) maximum strain, obtained from test b) Results are reported as mean value ± standard deviation. Statistical analysis was performed by one-way ANOVA followed by Bonferroni test with multiple comparisons. ($^{\circ}p < 0.01$, $^{\#}p < 0.001$, $^{\S}p < 0.0001$).

3.3. Microbiological studies

3.3.1. The antibacterial activity on planktonic growth

The quantitative determination of the antimicrobial activity of Ag-MBGs showed a dose-dependent variation in all tested bacterial strains' growth. In particular, the results indicated significantly lower absorbance values at the highest concentration tested (Fig. 4a, b) indicating the capacity to interfere with the viability of bacterial cells. Furthermore, even though an antimicrobial effect on both planktonic growths was evident, *S. aureus* seemed the most susceptible strain to the Ag-MBGs composite materials (Fig. 4a), meanwhile, the encapsulated Ag-MBGs proved slightly more efficient after 3 days with *P. aeruginosa*, indicating a potential controlled release (Fig. 4b).

Microbial cell viability followed the pattern of growth inhibition observed by spectrophotometric monitoring. PCL/Ag-MBGs significantly reduced the viability of *S. aureus* cells treated with 4 mg/mL when compared to the PCL only ($^{\S}p < 0.0001$), meanwhile for *P. aeruginosa,* PCL/Ag-MBG 80/20 was the most efficient in interfering with the cellular fitness and capacity to develop colonies (Fig. 4c, d).

3.3.2. The antibacterial activity on biofilm formation

The PCL/Ag-MBGs were tested for their consequences on the adherence ability of the tested bacterial strains, given the fact that the bacterial biofilms are considered the most successful and competitive expression of the prokaryotic genome [34]. In general, the inclusion of Ag-MBGs into the PCL matrix reduced the bacterial cells' capacity to colonize the substrates, probably by interfering with the *quorum sensing* mechanisms. Particularly, in terms of biofilm formation, Gram-negative strain used in the present study, *P. aeruginosa,* seemed to be the most sensitive to the substrates loaded with Ag-MBGs, with lower OD values (Fig. 4e) and with larger growth inhibition zones if compared to the neat and the ones developed on Gram-positive, *S. aureus* (Fig. 4f, g).

3.3.3. Disc diffusimetric method

The data obtained in disc diffusion test indicated an obvious zone of inhibition around the PCL/Ag-MBGs substrates, in the following order 90:10, 80:20, and 70:30 with the largest diameter of 20 mm obtained on the agar plate around PCL/Ag-MBG 90:10 (Fig. 4f, g).

3.4. Biological characterization

3.4.1. Cell viability

The biocompatibility of the composite substrates consisting of a PCL matrix and Ag-MBGs was studied *in vitro* adopting PDLSCs. Cell viability

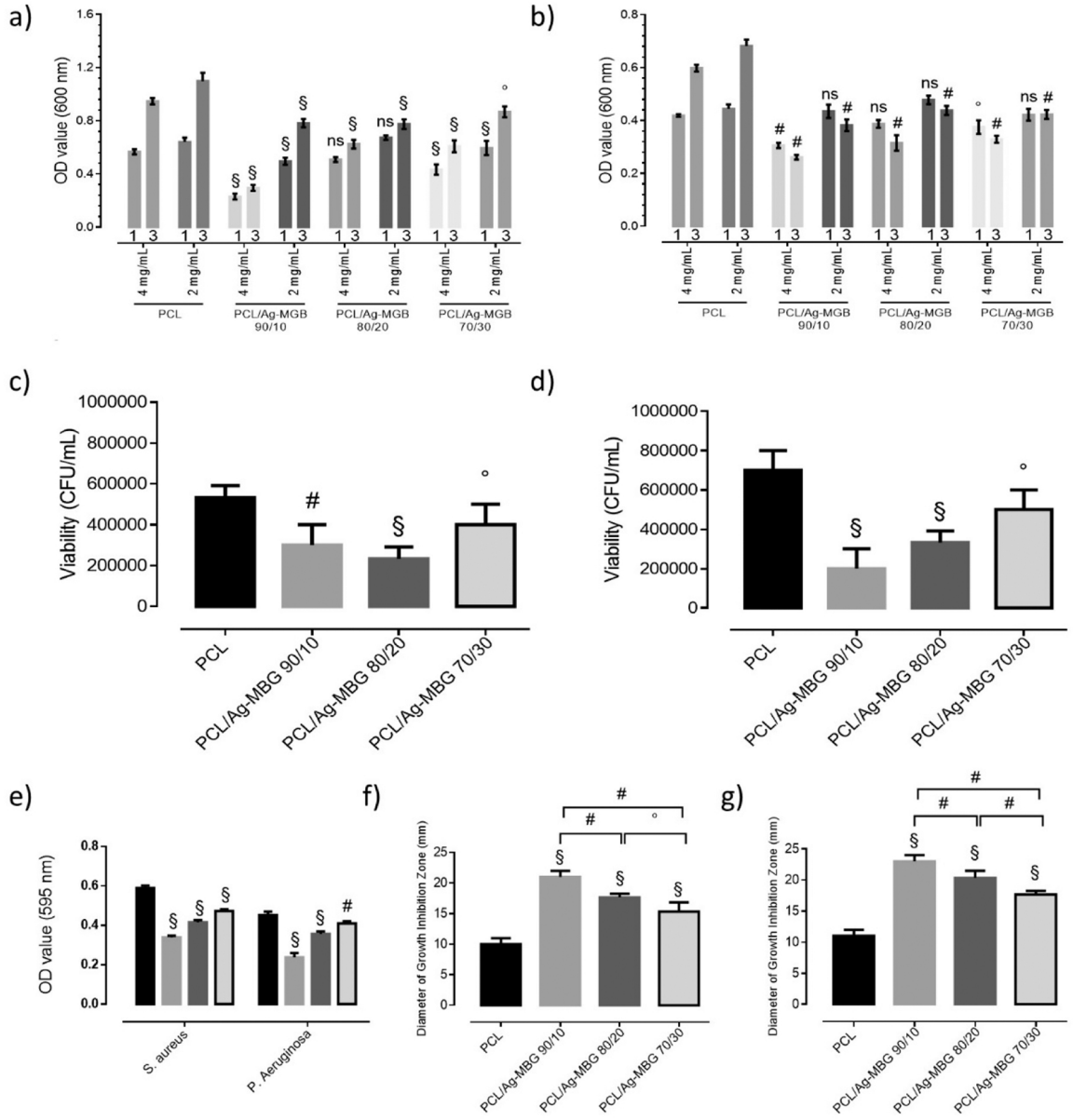

Fig. 4. Results from microbiological tests performed on Gram-positive, *S. aureus* (ATCC 25923) (a and c) and Gram-negative strains, *P. aeruginosa* (ATCC 27853) (b and d). a), b) Effect of different extract concentrations (2 and 4 mg/mL) on planktonic growth at 1 and 3 days. c), d) Bacterial viability (CFU/mL) at tested concentration 4 mg/mL at 1 day. e) Bacterial adherent growth of *S. aureus* and *P. aeruginosa* and diameter of microbial growth inhibition zone (mm) of f) *S. aureus* and g) *P. aeruginosa,* respectively. Results are reported as mean value ± standard deviation. Statistical analysis was performed by one-way (a-b, e-g) or two-way (c-d) ANOVA followed by Bonferroni test with multiple comparisons. ($^{\circ}p < 0.01$, $^{\#}p < 0.001$, $^{\S}p < 0.0001$).

was evaluated as the percentage of Alamar Blue reduction over the culture time. For each time point (1, 3, 7, 14, 21, and 28 days) the PCL/Ag-MBGs composites percentage of reduction of Alamar Blue was assessed and compared to the neat PCL ones (Fig. 5a). The results obtained from the Alamar Blue assay have evidenced that PDLSCs were viable on all the different formulations of PCL/Ag-MBGs composite substrates (PCL/Ag-MBG 90/10, PCL/Ag-MBG 80/20, PCL/Ag-MBG 70/30) over time, as the percentage of Alamar Blue reduction increased with time. It can be noticed that composites characterized by a concentration of 10% and 20% by weight of Ag-MBGs seemed to provide higher values of the percentage of Alamar Blue reduction over culture time if compared to the neat PCL substrates ($^{\S}p < 0.0001$). The above reported results confirmed that surface chemistry and topography could be fine-tuned by embedding Ag-MBGs fillers, thus intrinsically influencing hydrophilicity, cell viability, and proliferation.

3.4.2. Cell osteogenic differentiation: alkaline phosphatase expression

The ALP activity (U/gprot) at 7, 14, 21, and 28 days after cell seeding was evaluated. ALP is a well-established biomarker for the early osteogenic differentiation of cells and its measurement was used to assess the osteogenic expression of PDLSCs. The results showed the capability of all composite substrates to support the osteogenic differentiation of PDLSCs over time (Fig. 5b). Specifically, ALP assay showed that the composite with 30% by weight of Ag-MBGs (PCL/Ag-MBG 70/30) seemed to better promote the osteogenic differentiation if compared to the neat PCL ($^{\S}p < 0.0001$) and prolonged it more over time until 28 days from cell seeding. The obtained results suggested that the inclusion of 30% by weight of Ag-MBGs was able to provide and improve the long-term maintenance of PDLSCs osteogenic differentiation, stressing the importance of how the chemistry of Ag-MBGs particles and the different surface features can impact cell fate over time. The improvement of cell osteogenic differentiation over culture time could be correlated with the

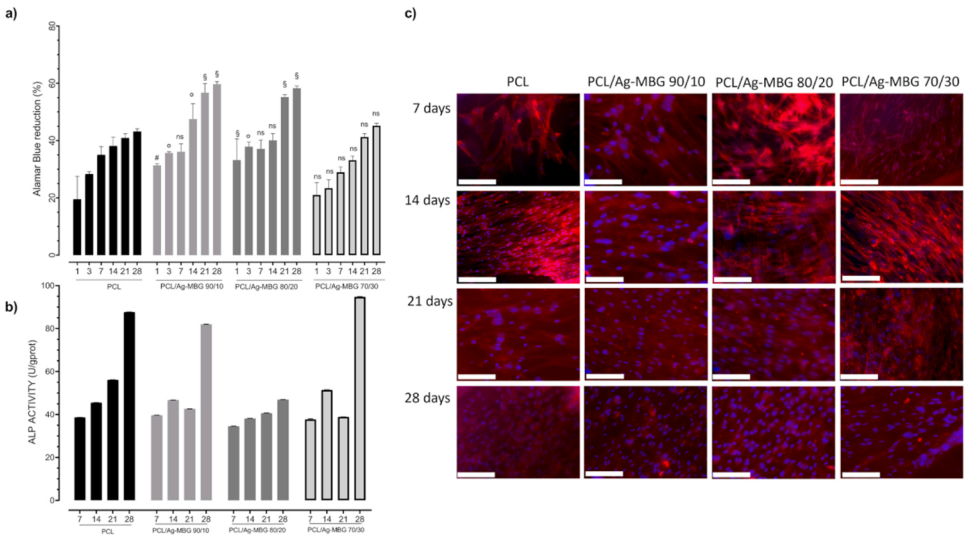

Fig. 5. a) Alamar blue reduction percentage at 1, 3, 7, 14, 21, and 28 days after seeding. Results are reported as mean value ± standard deviation. Statistical analysis was performed by two-way ANOVA followed by Bonferroni test with multiple comparisons. (ns, $^{\circ}p < 0.01$, $^{\#}p < 0.001$, $^{\S}p < 0.0001$); b) Data obtained from ALP assay at 7, 14, 21, and 28 days after cell seeding. Results are reported as mean value ± standard deviation. Statistical analysis was performed by two-way ANOVA followed by Bonferroni test with multiple comparisons. The values are all statistically significant compared to PCL at the same time ($^{\S}p < 0.0001$). c) Cell adhesion study: immunofluorescence images at various times after cell seeding. (Column I) From top to bottom, PCL at 7, 14, 21, and 28 days after cell seeding. (column II) From top to bottom, PCL/Ag-MBG 90/10 at 7, 14, 21, and 28 days after cell seeding. (column III) PCL/Ag-MBG 80/20 at 7, 14, 21, and 28 days after cell seeding. (column IV) PCL/Ag-MBG 70/30 at 7, 14, 21, and 28 days after cell seeding. Scale Bar: 125 μm. 20X objective. F-actin is in red, and nuclei in blue.

synergistic effect of substrate's mechanical properties, surface topography, and roughness as well as with composite biochemical composition, according to recent works' findings suggesting that substrates features strongly impact cell functions and fate through important and complex phenomena of mechanosensing and mechanotransduction [35,36].

3.4.3. *Cell morphology*

The immunofluorescence images allowed confirming the quantitative results obtained with Alamar Blue assay. Herein, the study performed on all the cell-laden substrates provided qualitative results in terms of PDLSCs adhesion and spreading at 7, 14, 21, and 28 days after seeding. Rhodamine phalloidin staining was used to visualize actin filaments and 4',6-diamidino-2-phenylindole (DAPI) for the nuclei. The results highlighted a homogenous cellular distribution on the surface, a good spreading, and a consequently narrow mesh cell network, with a slight increase of confluence in the PCL/Ag-MBG 80/20 at 28 days.

4. Discussions

The aim of the present study was to design and develop composite substrates consisting of a PCL matrix embedding Ag-MBGs. PCL was selected for its biocompatibility, biodegradability, and its physicochemical properties which have made it a suitable biomaterial for tissue-engineered scaffolds [37]. On the other hand, as already demonstrated in a previous work [21], Ag-MBGs highlighted a remarkable bioactivity and cytocompatibility, and antibacterial functionalities, along with interesting features for drug delivery and bone tissue engineering applications [20]. Furthermore, their nanostructure proved them as suitable candidates for the development of drug delivery systems [21]. However, for this field of application, Ag-MBGs alone and not embedded in a polymer matrix cannot be properly exploited. Indeed, due to their mesoporosity, MBGs possess low mechanical properties that limit their applications. Prompted by those positive results, the effects of the inclusion of Ag-MBGs, as an inorganic phase, on the morphological, mechanical, antibacterial and biological properties of a PCL-based matrix were assessed. Ag-MBGs were synthesized as already reported [20,21] and PCL/Ag-MBGs substrates were successfully produced by melting and molding technique.

Among the key properties of a biomaterial for bone tissue engineering applications, it is worth citing the mechanical behavior, which should be able to closely recapitulate the one of the natural tissues. Considering this aspect, in the design of composite biomaterials, it is of paramount importance to exactly balance the concentration of the inorganic phase embedded into the organic matrix. Indeed, it is well known that at the filler/matrix interface, stress concentration and discontinuities in the stress transfer mechanism may be due to the differences between the organic matrix and the inorganic fillers in terms of stiffness, hardness, and ductility. In addition, a high amount of fillers could have an adverse effect on mechanical performance, weakening the composite structure [31,32]. In particular, the results obtained from small punch tests suggested that beyond a threshold concentration, the Ag-MBGs functioned as "weak points" instead of reinforcement, since the mechanical properties of the composite substrates decreased. Accordingly to small punt tests, and other works in literature [38], the overall results highlighted that the mechanical behavior of the formulations containing a percentage of Ag-MBG higher than 10% by weight was negatively influenced by the presence of Ag-MBGs, even though the values of tensile modulus and maximum stress are still in the range of those found for hard tissues [39,40]. This effect could be ascribed to difficulties both in obtaining a homogeneous dispersion of Ag-MBGs into the PCL matrix and in its processing, given the increased material viscosity. However, a compromise among mechanical, antibacterial, and pro-regenerative features would be a desirable result, as higher MBGs concentrations should be preferred to improve the biological properties of the materials and to promote osteogenesis [38].

In this scenario, another crucial aspect to consider is achieving appropriate cell adhesion to the scaffold; however, this can be difficult with very hydrophobic scaffold matrices, such as PCL ones, which may lead to inadequate cell colonization. In the present work, the differences in water contact angle values between neat and composite substrates may result from a different surface topography, as well as surface composition, namely the presence and distribution of Ag-MBGs in the polymer matrix. Specifically, the above reported findings may be probably related to the synergistic contribution of both surface chemistry and topography that can be changed by embedding the inorganic

fillers [41]. Indeed, as PCL is a hydrophobic material, a value of the water contact angle higher than 90° was expected. In contrast to this, a water contact angle of 85.3 ± 4.1° was obtained for the neat PCL. This may be ascribed to the technique (melting and molding) employed for the preparation of the substrates, which can clearly alter the surface topography and roughness. Furthermore, in agreement with the results shown in other studies [42,43], BG particles, as a hydrophilic material, remarkably improve the hydrophilicity of the PCL matrix [44]. Other works reported that the reason for a change in contact angle could be that BG may cause a local increase of pH when dissolved, and hydroxide ions can accelerate the cleavage of ester linkages [45].

The development of biomaterials targeting regenerative medicine applications with antimicrobial properties that can resist bacterial contamination is highly needed. Implant-associated infections still represent a crucial clinical issue and a real burden, with a reported occurrence rate of 2–5% [46]. They are characterized by bacterial adhesion, colonization, and biofilm development. *S. aureus* is the most frequent bacterium responsible for infections of the bones and joints (70% of orthopedic implant infections) [46], including infections of prosthetic devices, and septic bursitis [47,48]. It is also responsible for 80–90% of pyogenic osteomyelitis cases [49], an inflammatory condition of the bone tissue caused by a microbial biofilm that can result in accelerated bone resorption and reactive bone formation. Furthermore, it is a hospital pathogen with a widespread, especially in surgery rooms [50]. Similarly, *P. aeruginosa* is a major pathogen that causes various infections [51]. Considering this issue, the health system is severely burdened by prosthetic infections, which necessitate lengthy hospital stays for antibiotic therapy, prosthesis removal, and replacement. Herein, either considering Gram-positive (*S. Aureus*) or Gram-negative (*P. Aeruginosa*), composites with the lowest Ag-MBGs concentration (PCL/Ag-MBG 90/10) showed the best behavior. This effect could be ascribed to the size of the Ag-MBGs, which, at higher concentrations, tend to cluster, as also reported by the morphological and mechanical analyses. It was reported that the smaller the particle sizes, the greater the antimicrobial effect [52]. Similar studies on different MBGs highlighted considerable antibacterial activity not only against *P. aeruginosa* and *S. aureus*, but also against diverse pathogens such as *E. coli*, *S. epidermidis*, *S. mutans,* and *E. coli* [29,53–55]. Herein, the two microbial strains used in the present study represent both groups of bacteria Gram-positive and Gram-positive, with specific adaptation and resistance mechanisms. For instance, the Gram-positive bacteria rely on the teichoic acids from the thick peptidoglycan layer for defense mechanisms against temperature, osmotic or toxic stresses, while the Gram-negative bacteria regulate the expression of porins within the outer membrane, thus limiting or even preventing the influx of drugs. Furthermore, Gram-negative pathogens were chosen due to their bacterial membranes, rich in phosphatidylethanol and phosphatidylglycerol [56]. It is suggested that Ag^+ ions react with and disrupt the function of bacterial cell membranes and crucial metabolic proteins and enzymes by binding to DNA and thiol groups in proteins [57]. However, the lack of agreement concerning the mechanism of action could be explained by the presence of multiple bactericidal mechanisms. The Ag^+ ions need to be considered too as an amount of cationic silver is released from the MBGs when in solution or after cell penetration. Furthermore, once the membrane barrier is disrupted, Ag^+ ions can lead to the release of reactive oxygen species (ROS), with the formation of free radicals, and powerful antimicrobial agents [25]. Another mechanism of action could be the ribosome denaturation and protein synthesis interference. Despite all those hypotheses, PCL substrates loaded with Ag-MBGs could be considered a viable alternative to antibiotherapy with the potential to control and prevent infections related to bone tissue disease (i.e. periodontitis), in agreement with other studies [58].

Finally, all the composite substrates had the ability to support PDLSCs adhesion and proliferation and to promote differentiation in the osteogenic sense. PDLSCs were adopted as cell sources for cell viability, proliferation, and differentiation assays since they represent a promising cellular approach for regenerative therapy in periodontium and maxillofacial bone. Recent studies have shown impactful results via PDLSCs in bone regeneration [59]. Indeed, it is well known that PDLSCs play a key role in periodontal homeostasis maintenance, as well as in the modulation of regeneration and remodeling of periodontal tissues [60–62].

5. Conclusion

Nowadays, different membranes are present on the market to guide periodontal tissue regeneration. Collagen is the most employed natural biomaterial (Bio-Gide® ED, Ossix® 3i, BioMend®), meanwhile Poly(DL-lactic acid) (EpiGuide®), Poly(DL-lactide-co-glycolide) (Resolut®), Polylactic acid (Guidor) and Poly(lactic-co-glycolic acid) (BioMesh) are used as synthetic polymers [63]. A few attempts have been made in the design of a PCL membrane reinforced with starch, calcium and silicon [64], with silica [65] or with calcium carbonate [66]. In the present work, a class of hybrid biomaterials with noticeably better physicochemical and mechanical characteristics, interesting antibacterial performances, and increased bioactivity and osteogenic potential were produced by combining Ag-MBGs with PCL.

A threshold concentration of Ag-MBGs (10% by weight) seemed to be sufficient in improving punching performances as well as the tensile Young's modulus, without negatively altering the tensile strength of the neat PCL. From a microbiological point of view, this concentration showed the best results highlighting a potential use in the treatment of bone-related infections, meanwhile cell viability and differentiation assays confirmed the PCL/Ag-MBGs composite substrates' ability to support PDLSCs over culture time.

The overall data suggest potential applications of the proposed PCL/Ag-MBGs composite substrates in maxillofacial bone and/or periodontal tissue repair. Indeed, PCL/Ag-MBGs could provide a valuable solution for significative critical conditions in which a simultaneous key role in regenerative and antibacterial processes is required (e.g., peri-implantitis treatments).

CRediT authorship contribution statement

Valentina Peluso: Conceptualization, Methodology, Validation, Investigation, Data Curation; **Ugo D'Amora:** Conceptualization, Methodology, Validation, Investigation, Data Curation, Project Administration; **Ana Maria Prelipcean:** Investigation, Data curation, Writing - Original draft preparation; **Stefania Scala:** Visualization, Investigation; **Nicola Gargiulo:** Resources, Supervision; **Ana-Maria Seciu-Grama:** Software, Validation, Formal Analysis; **Domenico Caputo:** Visualization, Writing - Reviewing and Editing; **Roberto De Santis:** Visualization, Writing - Review & Editing; **Antonio Gloria:** Methodology, Visualization, Writing - Review & Editing; **Teresa Russo:** Methodology, Formal analysis, Validation, Data curation, Writing, Supervision, Project administration.

Declaration of Competing Interest

The authors declare that they have no known competing financial interests or personal relationships that could have appeared to influence the work reported in this paper.

Data Availability

Data will be made available on request.

References

[1] P. Chocholata, V. Kulda, V. Babuska, Fabrication of scaffolds for bone-tissue regeneration, Materials 12 (2019) 568.
[2] A. Motameni, İ.S. Çardaklı, R. Gürbüz, A.Z. Alshemary, M. Razavi, Ö.C. Farukoğlu, Bioglass-polymer composite scaffolds for bone tissue regeneration: a review of

current trends, Int. J. Polym. Mater. Polym. Biomater. (2023) 1–20, https://doi.org/10.1080/00914037.2023.2186864.
[3] R. De Santis, A. Russo, A. Gloria, U. D'Amora, T. Russo, S. Panseri, M. Sandri, A. Tampieri, M. Marcacci, V.A. Dediu, C.J. Wilde, L. Ambrosio, Towards the design of 3D fiber-deposited poly(-caprolactone)/iron-doped hydroxyapatite nanocomposite magnetic scaffolds for bone regeneration, J. Biomed. Nanotechnol. 11 (2015) 1236–1246, https://doi.org/10.1166/jbn.2015.2065.
[4] M.N. Collins, G. Ren, K. Young, S. Pina, R.L. Reis, J.M. Oliveira, Scaffold fabrication technologies and structure/function properties in bone tissue engineering, Adv. Funct. Mater. 31 (2021), 2010609.
[5] G. Turnbull, J. Clarke, F. Picard, P. Riches, L. Jia, F. Han, B. Li, W. Shu, 3D bioactive composite scaffolds for bone tissue engineering, Bioact. Mater. 3 (2018) 278–314.
[6] U. D'Amora, A. Ronca, M. Raucci, S. Dozio, H. Lin, Y. Fan, X. Zhang, L. Ambrosio, In situ sol-gel synthesis of hyaluronan derivatives bio-nanocomposite hydrogels, Regenerative, Biomaterials 6 (2019) 249–258.
[7] R. De Santis, T. Russo, J.V. Rau, I. Papallo, M. Martorelli, A. Gloria, Design of 3D additively manufactured hybrid structures for cranioplasty, Materials 14 (2021) 181.
[8] T. Russo, V. Peluso, A. Gloria, O. Oliviero, L. Rinaldi, G. Improta, R. De Santis, V. D'Antò, Combination design of time-dependent magnetic field and magnetic nanocomposites to guide cell behavior, Nanomaterials 10 (2020) 577.
[9] P. Kesharwani, S.K. Prajapati, A. Jain, N. Mody, S. Sharma, A glimpse of biomedical application potential of biodegradable polymers for anticancer drug delivery, in: Polymeric Biomaterials for Healthcare Applications, Elsevier, 2022, pp. 211–234, https://doi.org/10.1016/B978-0-323-85233-3.00006-9.
[10] M. Dziadek, K. Dziadek, K. Checinska, B. Zagrajczuk, M. Golda-Cepa, M. Brzychczy-Wloch, E. Menaszek, A. Kopec, K. Cholewa-Kowalska, PCL and PCL/bioactive glass biomaterials as carriers for biologically active polyphenolic compounds: Comprehensive physicochemical and biological evaluation, Bioact. Mater. 6 (2021) 1811–1826.
[11] Z. Neščáková, H. Kaňková, D. Galusková, D. Galusek, A.R. Boccaccini, L. Liverani, Polymer (PCL) fibers with Zn-doped mesoporous bioactive glass nanoparticles for tissue regeneration, Int. J. Appl. Glass Sci. 12 (2021) 588–600.
[12] X. Yan, C. Yu, X. Zhou, J. Tang, D. Zhao, Highly ordered mesoporous bioactive glasses with superior in vitro bone-forming bioactivities, Angew. Chem. Int. Ed. 43 (2004) 5980–5984.
[13] R. Sergi, D. Bellucci, V. Cannillo, A review of bioactive glass/natural polymer composites: State of the art, Materials 13 (2020) 5560.
[14] F. Baino, E. Fiume, 3D printing of hierarchical scaffolds based on mesoporous bioactive glasses (MBGs)—Fundamentals and applications, Materials 13 (2020) 1688.
[15] M. Schumacher, P. Habibovic, S. van Rijt, Mesoporous bioactive glass composition effects on degradation and bioactivity, Bioact. Mater. 6 (2021) 1921–1931.
[16] D. Lozano, J. Gil-Albarova, C. Heras, S. Sánchez-Salcedo, V. Gómez-Palacio, A. Gómez-Blasco, J. Doadrio, M. Vallet-Regí, A. Salinas, ZnO-mesoporous glass scaffolds loaded with osteostatin and mesenchymal cells improve bone healing in a rabbit bone defect, J. Mater. Sci.: Mater. Med. 31 (2020) 1–11.
[17] A. Zambon, G. Malavasi, A. Pallini, F. Fraulini, G. Lusvardi, Cerium containing bioactive glasses: a review, ACS Biomater. Sci. Eng. 7 (2021) 4388–4401.
[18] M. Vallet-Regí, M. Colilla, I. Izquierdo-Barba, C. Vitale-Brovarone, S. Fiorilli, Achievements in Mesoporous Bioactive Glasses for Biomedical Applications, Pharmaceutics 14 (2022) 2636.
[19] H. Santos, J. Salonen, L. Bimbo, V.-P. Lehto, L. Peltonen, J. Hirvonen, Mesoporous materials as controlled drug delivery formulations, J. Drug Deliv. Sci. Technol. 21 (2011) 139–155.
[20] N. Gargiulo, I. De Santo, F. Causa, D. Caputo, P.A. Netti, Confined mesoporous silica membranes for albumin zero-order release, Microporous Mesoporous Mater. 167 (2013) 71–75.
[21] N. Gargiulo, A.M. Cusano, F. Causa, D. Caputo, P.A. Netti, Silver-containing mesoporous bioactive glass with improved antibacterial properties, J. Mater. Sci.: Mater. Med. 24 (2013) 2129–2135.
[22] X. Yan, G. Wei, L. Zhao, J. Yi, H. Deng, L. Wang, G.M. Lu, C. Yu, Synthesis and in vitro bioactivity of ordered mesostructured bioactive glasses with adjustable pore sizes, Microporous Mesoporous Mater. 132 (2010) 282–289.
[23] C. Wu, J. Chang, Y. Xiao, Mesoporous bioactive glasses as drug delivery and bone tissue regeneration platforms, Ther. Deliv. 2 (2011) 1189–1198.
[24] L. Zhao, X. Yan, X. Zhou, L. Zhou, H. Wang, J. Tang, C. Yu, Mesoporous bioactive glasses for controlled drug release, Microporous Mesoporous Mater. 109 (2008) 210–215.
[25] W. Fan, D. Wu, T. Ma, B. Fan, Ag-loaded mesoporous bioactive glasses against Enterococcus faecalis biofilm in root canal of human teeth, Dent. Mater. J. 34 (2015) 54–60.
[26] S. Kargozar, M. Montazerian, S. Hamzehlou, H.-W. Kim, F. Baino, Mesoporous bioactive glasses: Promising platforms for antibacterial strategies, Acta Biomater. 81 (2018) 1–19.
[27] T. Guo, K. Gulati, H. Arora, P. Han, B. Fournier, S. Ivanovski, Race to invade: Understanding soft tissue integration at the transmucosal region of titanium dental implants, Dent. Mater. 37 (2021) 816–831.
[28] A. Bagde, A. Kuthe, S. Quazi, V. Gupta, S. Jaiswal, S. Jyothilal, N. Lande, S. Nagdeve, State of the art technology for bone tissue engineering and drug delivery, Irbm 40 (2019) 133–144.
[29] Y. Wang, X. Chatzistavrou, D. Faulk, S. Badylak, L. Zheng, S. Papagerakis, L. Ge, H. Liu, P. Papagerakis, Biological and bactericidal properties of Ag-doped bioactive glass in a natural extracellular matrix hydrogel with potential application in dentistry, Eur. Cell Mater. 29 (2015) 342–355.
[30] A. Di Vito, A. Giudice, E. Chiarella, N. Malara, F. Bennardo, L. Fortunato, In vitro long-term expansion and high osteogenic potential of periodontal ligament stem cells: More than a mirage, Cell Transplant. 28 (2019) 129–139.
[31] T. Russo, A. Gloria, V. D'Antò, U. D'Amora, G. Ametrano, F. Bollino, R. De Santis, G. Ausanio, M. Catauro, S. Rengo, Poly (ϵ-Caprolactone) Reinforced with Sol-Gel Synthesized Organic-Inorganic Hybrid Fillers as Composite Substrates for Tissue Engineering, J. Appl. Biomater. Biomech. 8 (2010) 146–152.
[32] A. Gloria, T. Russo, U. d'Amora, S. Zeppetelli, T. d'Alessandro, M. Sandri, M. Bañobre-López, Y. Piñeiro-Redondo, M. Uhlarz, A. Tampieri, Magnetic poly (ε-caprolactone)/iron-doped hydroxyapatite nanocomposite substrates for advanced bone tissue engineering, J. R. Soc. Interface 10 (2013), 20120833.
[33] Z. Mousavi Nejad, A. Zamanian, M. Saeidifar, H.R. Vanaei, M. Salar, Amoli, 3D bioprinting of polycaprolactone-based scaffolds for pulp-dentin regeneration: investigation of physicochemical and biological behavior, Polymers 13 (2021) 4442.
[34] M. Khalid, M. Bilal, D. Huang, Role of flavonoids in plant interactions with the environment and against human pathogens—A review, J. Integr. Agric. 18 (2019) 211–230.
[35] S. Fusco, V. Panzetta, V. Embrione, P.A. Netti, Crosstalk between focal adhesions and material mechanical properties governs cell mechanics and functions, Acta Biomater. 23 (2015) 63–71, https://doi.org/10.1016/j.actbio.2015.05.008.
[36] Y. Hou, L. Yu, W. Xie, L.C. Camacho, M. Zhang, Z. Chu, Q. Wei, R. Haag, Surface Roughness and Substrate Stiffness Synergize To Drive Cellular Mechanoresponse, Nano Lett. 20 (2020) 748–757, https://doi.org/10.1021/acs.nanolett.9b04761.
[37] I. Rajzer, A. Kurowska, J. Frankova, R. Sklenářová, A. Nikodem, M. Dziadek, A. Jabłoński, J. Janusz, P. Szczygieł, M. Ziąbka, 3D-Printed Polycaprolactone Implants Modified with Bioglass and Zn-Doped Bioglass, Materials 16 (2023) 1061.
[38] Y. Kim, J.Y. Lim, G.H. Yang, J.-H. Seo, H.-S. Ryu, G. Kim, 3D-printed PCL/bioglass (BGS-7) composite scaffolds with high toughness and cell-responses for bone tissue regeneration, J. Ind. Eng. Chem. 79 (2019) 163–171.
[39] H. Qu, H. Fu, Z. Han, Y. Sun, Biomaterials for bone tissue engineering scaffolds: A review, RSC Adv. 9 (2019) 26252–26262.
[40] J.-W. Jang, K.-E. Min, C. Kim, J. Shin, J. Lee, S. Yi, Scaffold Characteristics, Fabrication Methods, and Biomaterials for the Bone Tissue Engineering, Int. J. Precis. Eng. Manuf. (2023) 1–19.
[41] M. Ramiasa-MacGregor, A. Mierczynska, R. Sedev, K. Vasilev, Tuning and predicting the wetting of nanoengineered material surface, Nanoscale 8 (2016) 4635–4642.
[42] A. Bruyas, F. Lou, A.M. Stahl, M. Gardner, W. Maloney, S. Goodman, Y.P. Yang, Systematic characterization of 3D-printed PCL/β-TCP scaffolds for biomedical devices and bone tissue engineering: Influence of composition and porosity, J. Mater. Res. 33 (2018) 1948–1959.
[43] F. Keivani, P. Shokrollahi, M. Zandi, S. Irani, F. Shokrolahi, S. Khorasani, Engineered electrospun poly (caprolactone)/polycaprolactone-g-hydroxyapatite nano-fibrous scaffold promotes human fibroblasts adhesion and proliferation, Mater. Sci. Eng.: C. 68 (2016) 78–88.
[44] M. Dziadek, B. Zagrajczuk, E. Menaszek, K. Dziadek, K. Cholewa-Kowalska, Poly (ε-caprolactone)-based membranes with tunable physicochemical, bioactive and osteoinductive properties, J. Mater. Sci. 52 (2017) 12960–12980.
[45] C. Bossard, H. Granel, Y. Wittrant, É. Jallot, J. Lao, C. Vial, H. Tiainen, Polycaprolactone/bioactive glass hybrid scaffolds for bone regeneration, Biomed. Glass 4 (2018) 108–122.
[46] J. Lin, N.-Y.T. Nguyen, C. Zhang, A. Ha, H.H. Liu, Antimicrobial properties of MgO nanostructures on magnesium substrates, ACS Omega 5 (2020) 24613–24627.
[47] R. Michels, K. Last, S.L. Becker, C. Papan, Update on coagulase-negative staphylococci—what the clinician should know, Microorganisms 9 (2021) 830.
[48] I. Atkinson, A.M. Seciu-Grama, S. Petrescu, D. Culita, O.C. Mocioiu, M. Voicescu, R.-A. Mitran, D. Lincu, A.-M. Prelipcean, O. Craciunescu, Cerium-containing mesoporous bioactive glasses (MBGs)-derived scaffolds with drug delivery capability for potential tissue engineering applications, Pharmaceutics 14 (2022) 1169.
[49] K.L. Urish, J.E. Cassat, Staphylococcus aureus osteomyelitis: bone, bugs, and surgery, Infect. Immun. 88 (2020) e00932–19.
[50] D. Barcudi, E.J. Sosa, R. Lamberghini, A. Garnero, D. Tosoroni, L. Decca, L. Gonzalez, M.A. Kuyuk, T. Lopez, I. Herrero, P. Cortes, M. Figueroa, A.L. Egea, P. Gagetti, D.A. Fernandez Do Porto, A. Corso, A.G. Turjanski, J.L. Bocco, C. Sola, MRSA dynamic circulation between the community and the hospital setting: New insights from a cohort study, J. Infect. 80 (2020) 24–37, https://doi.org/10.1016/j.jinf.2019.10.001.
[51] M.G. Wilson, S. Pandey, Pseudomonas aeruginosa, in: StatPearls, StatPearls Publishing, Treasure Island (FL), 2023. ⟨http://www.ncbi.nlm.nih.gov/books/NBK557831/⟩ (accessed October 6, 2023).
[52] M. Qasim, N. Udomluck, J. Chang, H. Park, K. Kim, Antimicrobial activity of silver nanoparticles encapsulated in poly-N-isopropylacrylamide-based polymeric nanoparticles, Int. J. Nanomed. 13 (2018) 235.
[53] J. Pratten, S.N. Nazhat, J.J. Blaker, A.R. Boccaccini, In vitro attachment of Staphylococcus epidermidis to surgical sutures with and without Ag-containing bioactive glass coating, J. Biomater. Appl. 19 (2004) 47–57.
[54] K. Chotchindakun, J. Pekkoh, J. Ruangsuriya, K. Zheng, I. Unalan, A.R. Boccaccini, Fabrication and characterization of cinnamaldehyde-loaded mesoporous bioactive glass nanoparticles/PHBV-based microspheres for preventing bacterial infection and promoting bone tissue regeneration, Polymers 13 (2021) 1794.
[55] M. Bellantone, H.D. Williams, L.L. Hench, Broad-spectrum bactericidal activity of Ag2O-doped bioactive glass, Antimicrob. Agents Chemother. 46 (2002) 1940–1945.

[56] M. Taniguchi, A. Ochiai, K. Takahashi, S. Nakamichi, T. Nomoto, E. Saitoh, T. Kato, T. Tanaka, Antimicrobial activity against Porphyromonas gingivalis and mechanism of action of the cationic octadecapeptide AmyI-1-18 and its amino acid-substituted analogs, J. Biosci. Bioeng. 122 (2016) 652–659.
[57] M. Diba, A. Boccaccini, Silver-containing bioactive glasses for tissue engineering applications, in: Precious Metals for Biomedical Applications, Elsevier, 2014, pp. 177–211.
[58] S.R. Gavinho, A.S. Pádua, I. Sá-Nogueira, J.C. Silva, J.P. Borges, L.C. Costa, M.P. F. Graça, Fabrication, Structural and Biological Characterization of Zinc-Containing Bioactive Glasses and Their Use in Membranes for Guided Bone Regeneration, Materials 16 (2023) 956.
[59] Z. Zhao, J. Liu, M.D. Weir, A. Schneider, T. Ma, T.W. Oates, H.H. Xu, K. Zhang, Y. Bai, Periodontal ligament stem cell-based bioactive constructs for bone tissue engineering, Front. Bioeng. Biotechnol. 10 (2022).
[60] I. Rexhepi, M. Paolantonio, L. Romano, M. Serroni, P. Santamaria, L. Secondi, G. Paolantonio, B. Sinjari, P. De Ninis, B. Femminella, Efficacy of inorganic bovine bone combined with leukocyte and platelet-rich fibrin or collagen membranes for treating unfavorable periodontal infrabony defects: Randomized non-inferiority trial, J. Periodontol. 92 (2021) 1576–1587.
[61] C. Zhang, Y. Lu, L. Zhang, Y. Liu, Y. Zhou, Y. Chen, H. Yu, Influence of different intensities of vibration on proliferation and differentiation of human periodontal ligament stem cells, Arch. Med. Sci. 11 (2015) 638–646.
[62] V. Peluso, L. Rinaldi, T. Russo, O. Oliviero, A. Di Vito, C. Garbi, A. Giudice, R. De Santis, A. Gloria, V. D'Antò, Impact of magnetic stimulation on periodontal ligament stem cells, Int. J. Mol. Sci. 23 (2021) 188.
[63] P.S. Babo, R.L. Pires, R.L. Reis, M.E. Gomes, Membranes for periodontal tissues regeneration, Ciência Tecnol. Dos. Mater. 26 (2014) 108–117, https://doi.org/10.1016/j.ctmat.2015.03.007.
[64] J.F. Requicha, T. Moura, I.B. Leonor, T. Martins, F. Muñoz, R.L. Reis, M.E. Gomes, C.A. Viegas, Evaluation of a starch-based double layer scaffold for bone regeneration in a rat model, J. Orthop. Res. 32 (2014) 904–909, https://doi.org/10.1002/jor.22609.
[65] E.-J. Lee, S.-H. Teng, T.-S. Jang, P. Wang, S.-W. Yook, H.-E. Kim, Y.-H. Koh, Nanostructured poly(ε-caprolactone)–silica xerogel fibrous membrane for guided bone regeneration, Acta Biomater. 6 (2010) 3557–3565, https://doi.org/10.1016/j.actbio.2010.03.022.
[66] K. Fujihara, M. Kotaki, S. Ramakrishna, Guided bone regeneration membrane made of polycaprolactone/calcium carbonate composite nano-fibers, Biomaterials 26 (2005) 4139–4147, https://doi.org/10.1016/j.biomaterials.2004.09.014.